JOURNAL OF MATERIALS SCIENCE 28 (1993) 677–683

Secondary and tertiary dendrite arm spacing relationships in directionally solidified Al–Si alloys

R. N. GRUGEL
Center for Microgravity Research and Applications, Vanderbilt University, Box 6079-B, Nashville, TN 37235, USA

Secondary, λ_2, and tertiary, λ_3, dendrite arm spacings have been measured from Al–Si alloys which were directionally solidified as functions of growth velocity, V, temperature gradient, G, and composition, C_0. Both λ_2 and λ_3 decreased as the imposed growth velocity and silicon concentrations were increased, and for each function a systematic variance in the rate was seen. Complications with measuring secondary arm spacings are shown and it was found that the tertiary arm data agree much better with coarsening theory, the implication being that λ_3, when measurable, is a more representative and reliable measure of the solidification history than λ_2.

1. Introduction

While the strength and ductility of a casting is generally attributed to continuous primary dendrites, λ_1, the spacing between secondary, λ_2, and tertiary, λ_3, arms can effectively serve to isolate potentially detrimental eutectic or intermetallic phases and thus contribute to the product's overall integrity. Individual contributions depend in part on the distribution, volume fraction, and relative scale of these microstructural constituents, an idea of which may be gained from Fig. 1a and b which show λ_1, λ_2 and λ_3 as functions of the imposed growth velocity and composition.

The examination of quenched interfaces in metallic systems [1–8] and direct observation in transparent, organic analogue systems [9–20] have shown secondary arms to initiate at a distance shortly behind the dendrite tip with an initial spacing, $\lambda_2' \approx 2R$, where R is the dendrite tip radius. Under conditions of steady-state growth the primary dendrite spacing, λ_1, does not change. Secondary arms, however, are seen to rapidly coarsen in the mushy region and consequently their spacing changes considerably along the primary trunk prior to being frozen-in by, for example, a terminal eutectic reaction. A model describing this coarsening was proposed by Kattamis, *et al.* [21] and has since been followed by a number of others [22–29]. In addition to coarsening, Allen and Hunt [11] showed that the imposed temperature gradient influenced interdendritic solute redistribution and promoted secondary dendrite arm migration up the primary stalk, a point which has recently received more attention [30, 31].

Tertiary dendrite arms, by definition, initiate from secondary branches. The only previous investigation of λ_3 spacings found was that of Taha [32] who noted a spacing–growth rate relationship and suggested the need for further studies. Tertiary arms have also been observed to grow past initiating secondary branches and go on to become primary dendrites [17, 33].

2. Experimental procedure and results

This study utilized aluminium (99.99% major impurity 0.003% Fe)–silicon (99.999%) alloys ranging in composition from 4–12 wt % Si. Silicon was added to molten aluminium, vigorously stirred, and cast into 6 mm diameter rods which were then machined to accommodate the 5 mm i.d. alumina tubes used in the directional solidification experiments. The samples were lowered vertically downward through a Bridgman type furnace with thermal data being provided by two fine Pt/Pt–10% Rh thermocouples, separated by 5 mm and protected by alumina sheathing, which were inserted directly into the molten alloy. After ~ 70 mm directional solidification, the growth front was interrupted by dropping the sample into a water spray (cooling rate $\sim 100\ K\ s^{-1}$). The samples were then sectioned by a thin diamond-impregnated blade and mounted in an epoxy resin. Sample preparation consisted of a standard series of wet grinding and polishing, followed by etching in a solution of 60 ml H_2O, 10 g NaOH, and 5 g $K_3Fe(CN)_6$ for ~ 10 s.

Fig. 2 is a representative micrograph of a longitudinal section from which secondary dendrite arm spacing, λ_2, measurements were made. Closer examination of Fig. 2 suggests two possibilities for measuring the spacing. The first (▲) is to include all branches, regardless of stature, that are associated with the primary trunk. These symbols in caption represent an average

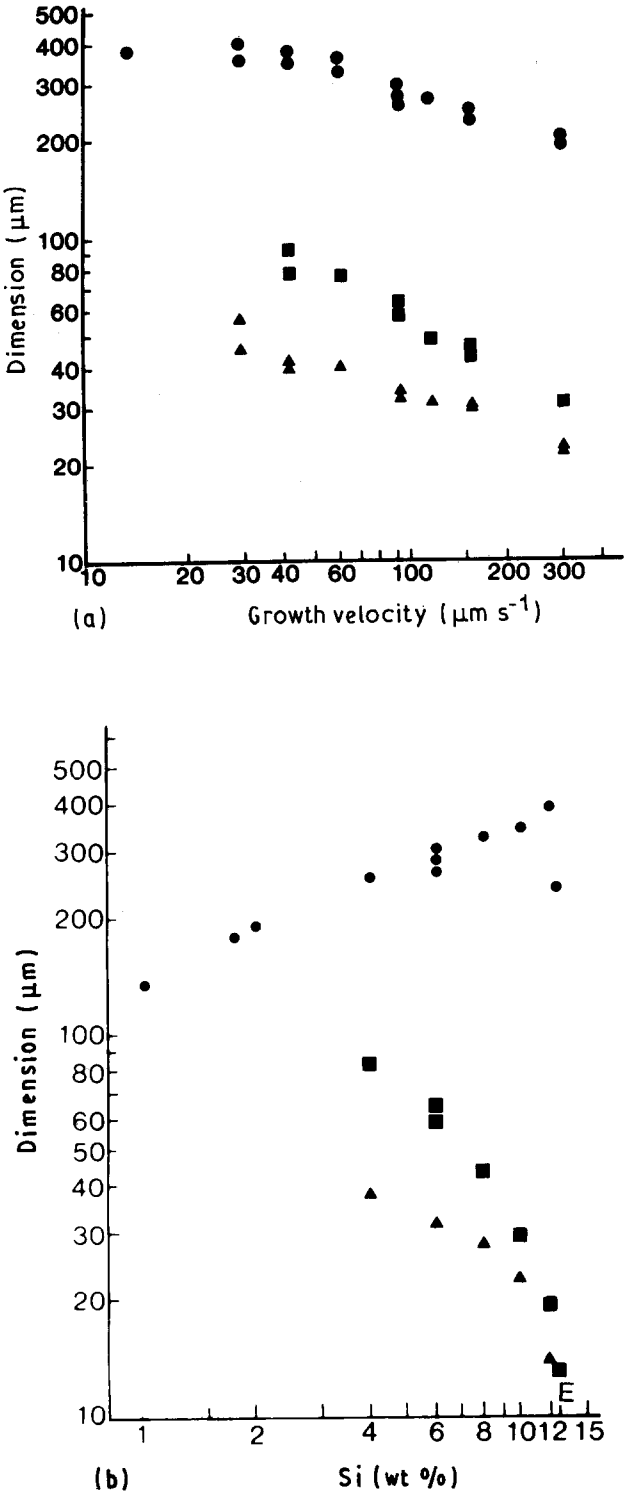

Figure 1 (●) Primary (λ_1), (■) secondary (λ_2), and (▲) tertiary (λ_3) dendrite arm spacing relationships (a) as a function of the imposed growth velocity, for Al-6 wt % Si; and (b) as a function of silicon concentration, "E" denotes the eutectic, 12.6 wt % Si, $V = 93\ \mu m\ s^{-1}$, $G = 15\ K\ mm^{-1}$.

spacing of ~23 μm. The second case (●) only includes those, termed "active" [13, 14], which are seen to have grown ahead of those previously included, and have a spacing of ~33 μm. Clearly some judgement is required when making these measurements and the λ_2 spacings reported here have been measured by the latter method as these branches obviously dominate and will influence material properties to a much greater extent than their degenerate neighbours. The data represent the average as determined from at least five

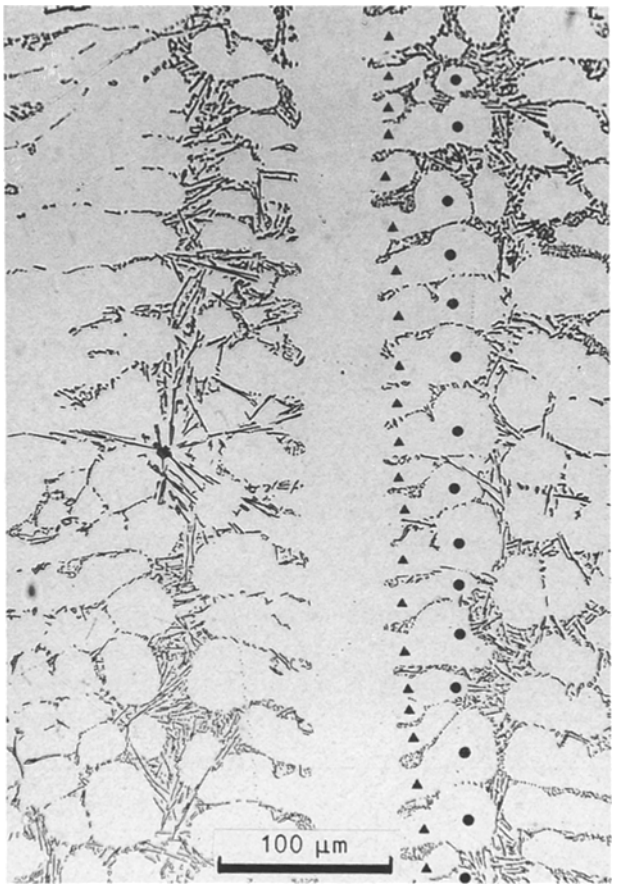

Figure 2 Longitudinal micrograph of an Al–6 wt % Si alloy which shows two possibilities for measuring the secondary arm spacing (λ_2). (▲) All arms, (●) active arms [13, 14], the latter constituting the reported spacing. Imposed growth velocity = 301 $\mu m\ s^{-1}$, temperature gradient = 15 $K\ mm^{-1}$.

measurements on a given section, the deviation about this mean value being some 9%. While vestiges of secondary arms could be seen in samples solidified at slow growth rates and/or with low silicon concentrations, e.g. 2 wt %, no meaningful measurements could be made. Measurements of the secondary dendrite arm spacings as functions of growth velocity and composition are, respectively, shown in Fig. 3a and b.

In contrast to secondary branches, determining the tertiary dendrite arms for spacing measurements, λ_3, was relatively unambiguous, as may be appreciated by examining Fig. 4 which is indicative of the solidification microstructures when viewed in cross-section. Here the average spacing as determined from 10–20 measurements is reported, the cumulative standard deviation about this mean being ~10%. The measured tertiary dendrite arm spacings as a function of the imposed growth velocity and composition are shown, respectively, in Fig. 5a and b.

3. Discussion

3.1. Secondary dendrite arm spacing

There have been many studies which reported secondary dendrite arm spacing measurements as a function of some solidification parameter [2, 34–46]. Often this parameter was defined to be the cooling rate [34,

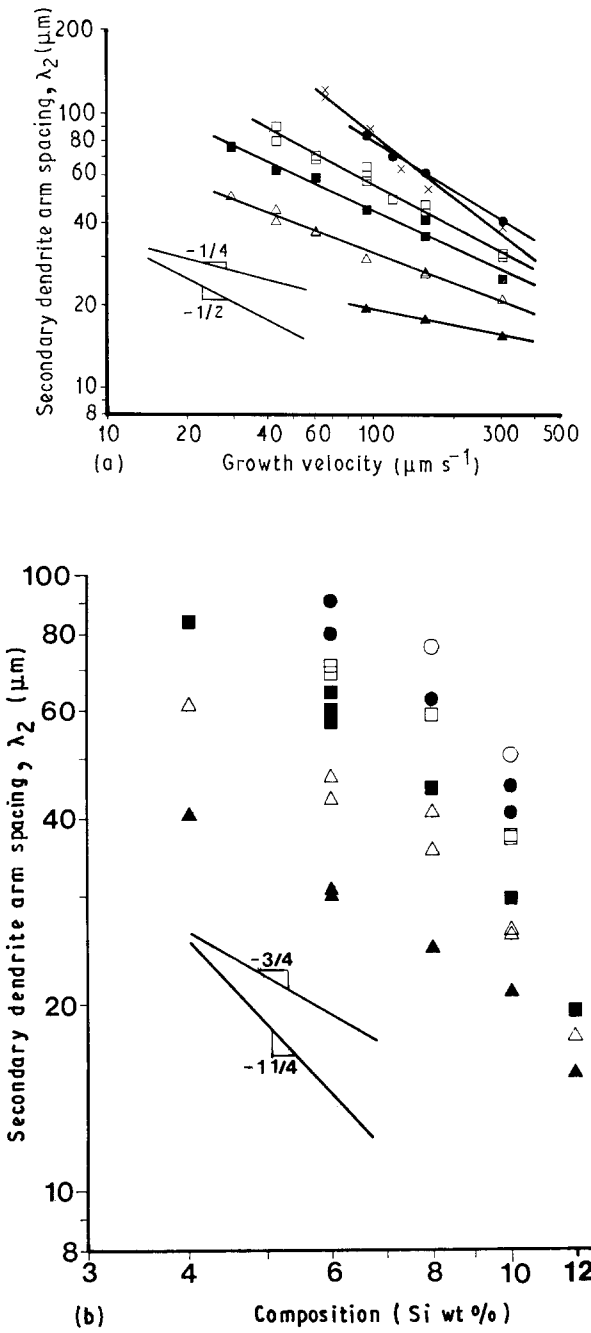

Figure 3 Secondary dendrite arm spacing (λ_2) as a function of (a) the imposed growth velocity for silicon concentrations (●) 4, (□) 6, (■) 8, (△) 10, (▲) 12 wt % at $G = 15$ K mm^{-1}, and (×) 6 wt % at $G = 5$ K mm^{-1}; and (b) silicon composition for growth velocities (○) 29.2, (●) 43, (□) 60.3, (■) 93.6, (△) 156.1, (▲) 301.1 μm s^{-1}, $G = 15$ K mm^{-1}.

TABLE I Comparison of the exponents measured according to the relationship, $\lambda_2 = KV^{-n}$ for several alloy systems

System	Exponent, $-n$	Reference
Pb–5 at % Sb	~0.48–~1.1	[40]
Al–(2.8–8.4 wt %)Si	~0.25	[41]
Fe–(0.59 and 1.48% C)	0.37–0.5	[42]
Zn–(6, 5, 8 and 11 wt %)Al	0.32–0.42	[47]

36–38, 40, 42, 45], which consequently implies continually changing growth rates and temperature gradients at the solidification interface. Thus while linear relationships were found between λ_2 spacing and cooling rate, the individual contributions of V, G and,

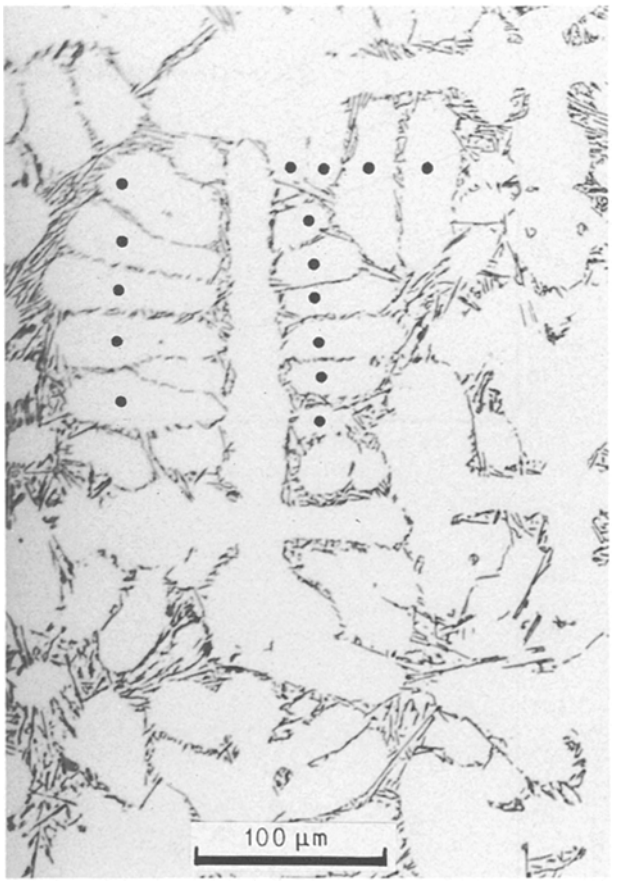

Figure 4 Typical cross-sectional micrograph of an Al–6 wt % Si alloy from which the tertiary dendrite spacing (●) was determined. Imposed growth velocity = 301 μm s^{-1}, temperature gradient = 15 K mm^{-1}.

to some extent, C_0 could not be ascertained. Secondary arm spacing as functions of V, G and C_0 have also been shown [39–42, 46], however, outside of exhibiting general trends, there appears to be little correlation when the results of different studies are compared. For example, it is convenient to relate the measured secondary arm spacing to the imposed growth rate, V, as

$$\lambda_2 = KV^{-n} \quad (1)$$

where K is a proportionality constant.

When a number of studies was evaluated, considerable variation in the exponent was found, as is evident in Table I. Here exponents are seen to range from -0.32 to -1.1. Further examination reveals a change in n at constant composition in one case [39], and then no change in n for several compositions [40]. These discrepancies may, in part, be attributed to varying processing parameters, e.g. temperature gradient, both within a given system and in comparison to others. In view of the complex interactions to which secondary arms are subject after their initiation, and the ambiguity in measuring them, it is perhaps naive to expect "n" to be constant. This, however, cannot be determined from the previous studies.

Consider now Fig. 3a which plots the measured secondary dendrite arm spacings as a function of imposed growth velocity for Al–(4–12 wt %) Si alloys. For a temperature gradient of 15 K mm^{-1}, the slope is

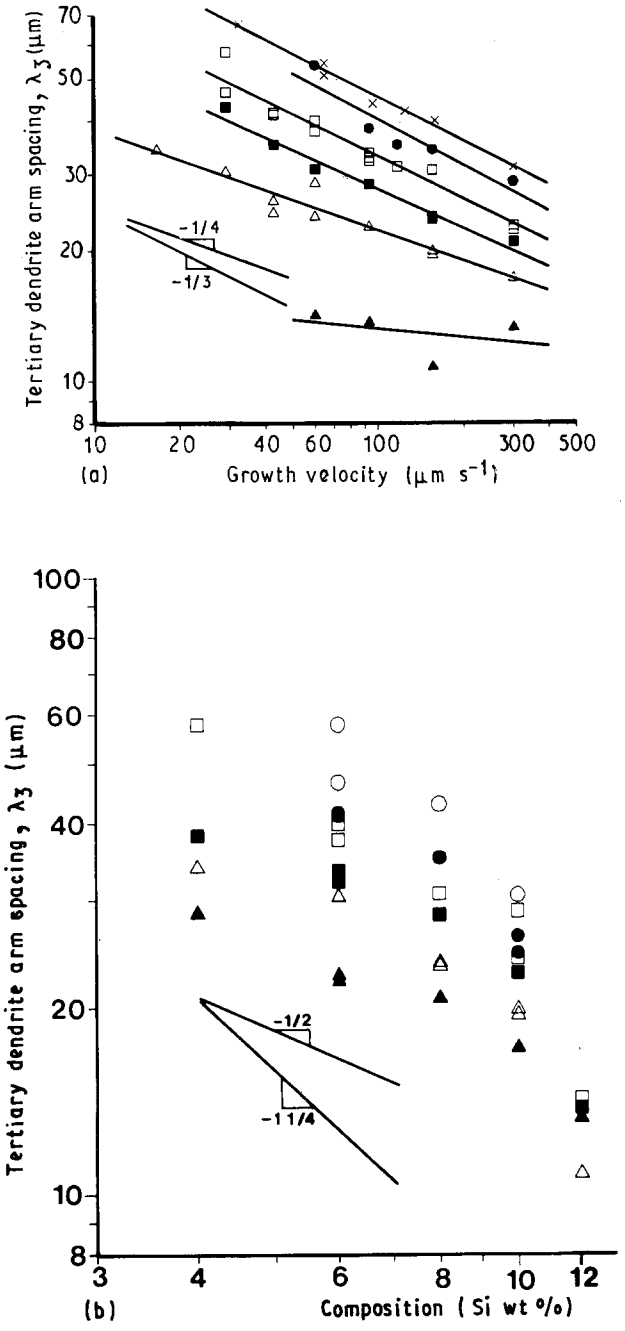

Figure 5 Tertiary dendrite arm spacing (λ_3) as a function of (a) the imposed growth velocity for several silicon concentrations, and (b) silicon composition for several growth velocities. For keys, see Fig. 3.

seen to decrease from slightly less than $-1/4$ to somewhat more than $-1/2$ as the silicon content is decreased from 12 to 4 wt %; the greatest, -0.71, being that of the 6 wt % alloy where $G = 5$ K mm^{-1}. This is in contradiction to the previous work with Al–Si alloys [41], but can be rationalized with the aid of Table II and observations from other studies.

Table II gives the equilibrium freezing range, $\Delta T'$ (liquidus temperature, T_L – eutectic temperature, T_E) for the silicon compositions employed in this study. From this, neglecting undercoolings, and with the measured temperature gradients, G, and growth velocities, V, the local solidification time, t_f, or time available for coarsening in the mushy zone can be calculated as

$$t_f = \Delta T'/GV \quad (2)$$

TABLE II Equilibrium freezing ranges for selected Al–Si alloys [47]

Si (wt %)	$\Delta T'$ (K)
4	59.2
6	47.2
8	31.6
10	14.1
12	4.8

TABLE III Calculation of the local solidification time, t_f, and length of the mushy zone, L_m, for some solidification conditions

Si (wt %)	G (K mm^{-1})	V(μm s^{-1})	t_f (s)	L_m (mm)
12	15	300	1.1	0.32
6	15	30	104.8	3.15
6	5	30	314.7	9.44

From this relationship it is easily deduced that secondary arms in low silicon concentration alloys growing at slow velocities spend more time in the mushy zone than those with high concentrations and fast growth rates, Table III. To put this further in perspective, the equilibrium length of the mushy zone, L_m, i.e. the distance from the dendrite tip to the eutectic horizontal, has also been calculated ($L_m = \Delta T'/G$).

Table III shows a considerable range between the calculated values of t_f and L_m for the solidification parameters employed in this study. Allen and Hunt [48] divided the dendritic region into two zones; an initial transient and a second termed quasi-stationary. The initial transient is prominent just behind the dendritic front and extends until the solute diffusion fields from adjacent dendrites overlap. This region can extend from the dendrite tips to the eutectic reaction (which essentially freezes in the microstructure) under solidification conditions of fast growth rates and/or high silicon concentrations [49]. This zone is further characterized by a rapid and dynamic increase in the solid volume fraction. Conversely, with low growth rates and/or low silicon concentrations the initial transient may only extend along a small fraction of the dendrite trunk before ceding to the quasi-stationary zone which is a rather stagnant region characterized by dendrite thickening. Thus, depending on the solidification conditions, the secondary arms are subject to development in extremely different environments. Consequently, considering the contribution to coarsening which must occur in the quasi-stationary region, one might expect an incremental increase in the λ_2 spacing as the growth velocity is decreased, and as the silicon composition is decreased. This is in accordance with the measurements of Fig. 3a and b and the earlier implications of Sharp and Hellawell [50].

A coarsening phenomenon has been previously evaluated by plotting the measured secondary dendrite arm spacing as a function of the local solidification time [2, 21, 40–44, 46]. Straight-line relationships have been reported when the data are plotted on log–log scales with the corresponding slopes found to

range from 0.3–0.5. The data of this study are similarly plotted in Fig. 6, and it is noted that the line equation, $\lambda_2 = 10t_f^{1/2}$, is included for comparative purposes only and is not fit to the data. While a linear regression analysis could very easily, and apparently successfully, be applied, it is felt this would compromise the results of Fig. 3a and b which show the consequence of processing parameters in conjunction with the complications arising from the extent of very different zones of solidification behaviour along the dendrite trunk. Thus, for a small t_f (fast growth rates and high silicon concentrations) the slope can be envisioned as $\approx 1/3$. The 6 wt % Si, $G = 5\ \mathrm{K\,mm^{-1}}$, data (○) exemplifies the opposite conditions (low growth rates and a considerably longer mushy zone) and subsequently a slope of ≈ 0.8. Another factor which will further complicate any analysis of λ_2 spacing is the contribution from secondary arm migration up the temperature gradient [11].

3.2. Tertiary dendrite arm spacing

The measured tertiary dendrite arm spacings are plotted in Fig. 5a and b as, respectively, functions of the imposed growth velocity and composition. Although the relative slopes differ somewhat, when compared to the λ_2 measurements of Fig. 3a and b, the same incremental trends are seen. Recalling the lack of ambiguity in making λ_3 measurements, comparison of Figs 3 and 5 gives credence to the assertion of only considering "active" branches when determining the secondary dendrite arm spacing. Furthermore, the claim of the dendritic field being subjected to two distinct and very different regimes of solidification behaviour is substantiated by examination of Fig. 7. Here the tertiary dendrite arm spacing has been measured from a series of cross-sectional micrographs taken through the mushy zone, i.e. from just past the dendrite tip and into the terminal eutectic, of a solid–liquid interface that had been quenched-in during growth. When λ_3 is plotted as a function of distance from the dendrite tip the spacing is initially seen to rapidly increase from ~5 to 30 μm, and then rises slowly. As a reference, the calculated [49] transition from the initial transient to the quasi-stationary zone [48] is also indicated. The point to be made here is that λ_3 (and by analogy, λ_2) can be viewed to evolve at two distinct rates. Thus, depending on the solidification parameters associated with a given alloy system, the tertiary arms may never evolve past the first zone before being frozen-in by the eutectic reaction, or, in contrast, they could spend a much greater percentage of time in the quasi-stationary zone. Consequently, as seen in Figs 3 and 5, it should be expected that the slopes of the data change, and in a consistent manner.

The tertiary dendrite arm spacing, λ_3, is plotted as a function of local solidification time, t_f, in Fig. 8. As in Fig. 6, the line equation, $\lambda_3 = 10t_f^{1/3}$, is not based on any analysis of the data. Note, however, that outside of small values of t_f, as might be expected in view of the above discussion, the fit is not unreasonable. In contrast to Fig. 6, not only are the 6 wt % Si, $G = 5\ \mathrm{K\,mm^{-1}}$ data in agreement with the others, but the slope of 1/3 is in accordance with coarsening theory. Although a number of factors certainly contribute, a first step toward resolving the difference found between Figs 6 and 8 ($\lambda_2 \propto t_f^{1/2}$ and $\lambda_3 \propto t_f^{1/3}$) might be taken by considering the imposed temperature gradient. Directional solidification techniques are employed with the intent of having dendrites grow opposite to the heat-flow direction in an aligned manner as constrained by the temperature gradient. In this respect, growth of the secondary branches is essentially perpendicular to the heat flow direction and, consequently, the arms are all at different temperatures. In contrast, while the temperature of the tertiary arms will drop as solidification continues, the

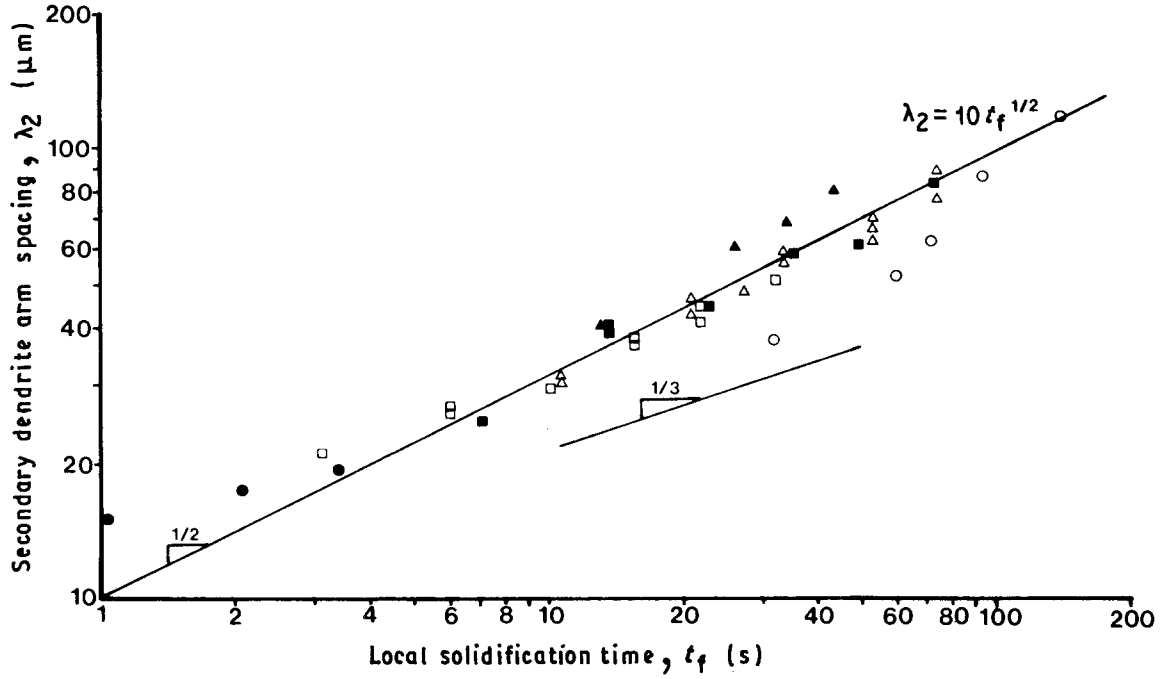

Figure 6 Plot of the measured secondary dendrite arm spacings, λ_2, as a function of local solidification time, t_f. Silicon concentrations wt % (▲) 4, (△) 6, (■) 8, (□) 10, (●) 12, G = 15 K mm^{-1}; (○) 6, G = 5 K mm^{-1}.

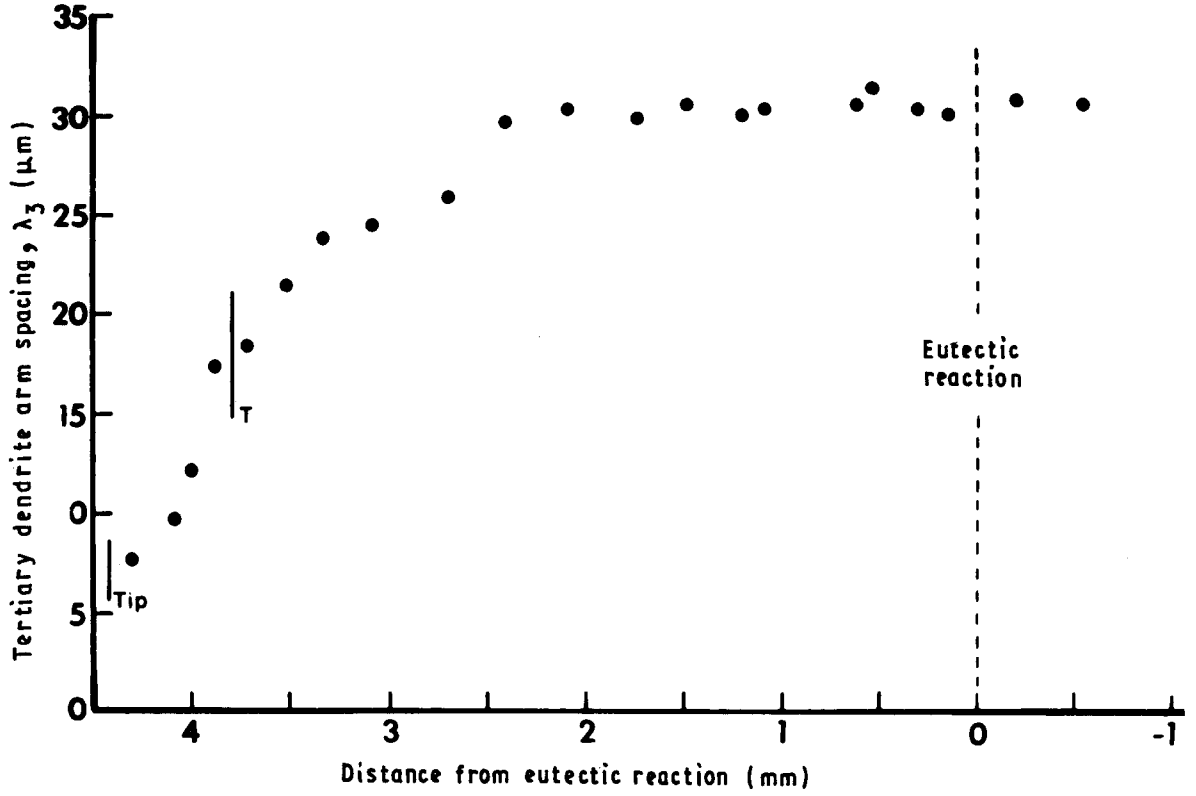

Figure 7 Plot of the measured tertiary dendrite arm spacings, λ_3, as a function of distance behind the dendrite tips. The calculated transition from the initial transient to the quasi-stationary zone is denoted by "T". Al–6 wt % Si, imposed growth velocity = 156 μm s^{-1}, temperature gradient = 15 K mm^{-1}.

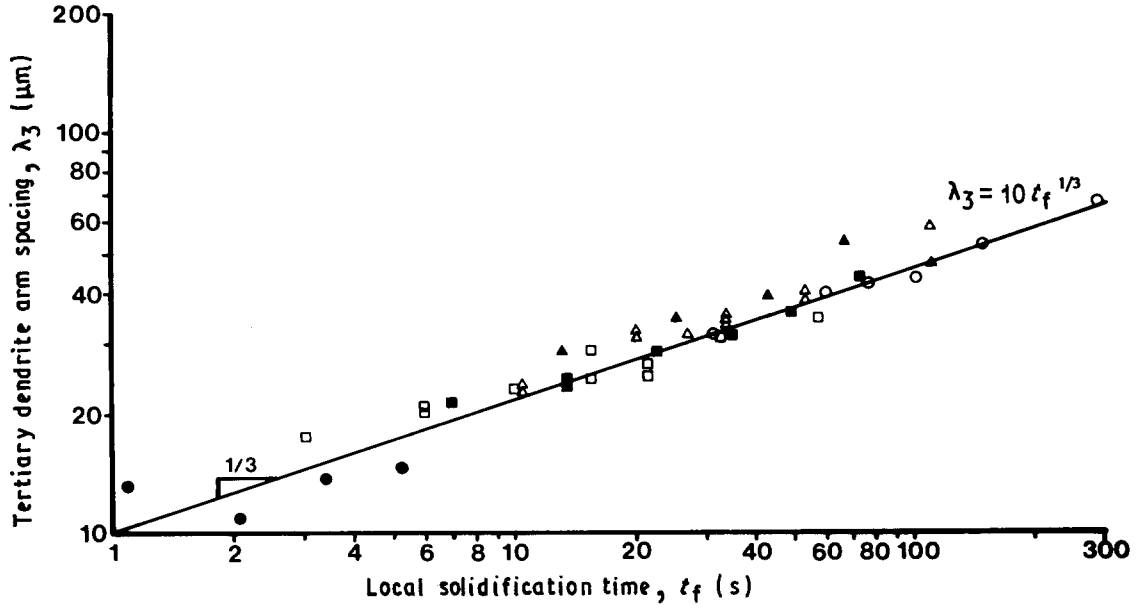

Figure 8 Plot of the measured tertiary dendrite arm spacings, λ_3, as a function of local solidification time, t_f. For key, see Fig. 6.

individual arms emanating off a given secondary branch may be envisioned as occupying an isothermal plane and coarsen accordingly. In this respect it might be concluded that movement of the secondary arms up the temperature gradient plays a major role towards establishing the final spacing while at the same time effectively disrupting the coarsening $t^{1/3}$ relationship.

4. Conclusions

1. Secondary and tertiary dendrite arm spacings were both found to decrease as a function of increasing growth velocity for a given composition. The rate of decrease, $d\lambda_{2,3}/dV$, was found to serially increase as the silicon concentration was decreased. The spacings also decreased as a function of increasing silicon concentration for a constant imposed growth rate.

The rate of decrease, $d\lambda_{2,3}/dC_0$, serially increased as the growth velocity decreased. The difference in rates is attributed to the existence of two fields in the mushy zone. Rapid coarsening of the branches occurs just behind the dendrite tips, and then rather abruptly transfers to a region where the spacing slowly increases; the relative contribution of each depends on the solidification parameters.

2. Coarsening of secondary arms was found, in general, to be proportional to time$^{1/2}$. For tertiary arms, time$^{1/3}$ behaviour was found. The deviation of the secondary spacing from $t^{1/3}$ has been attributed to secondary dendrite arm migration up the imposed temperature gradient.

3. The difficulties expressed in measuring secondary dendrite arm spacings as compared to tertiary, suggest the latter, when present, to be better representatives of the solidification conditions.

Acknowledgements

The author thanks Professor W. Kurz, Swiss Federal Institute of Technology, Lausanne, Switzerland, for providing laboratory facilities, and the collaboration of M. Gremaud is acknowledged. This research was supported by the Swiss National Foundation for Scientific Research and the NASA Office of Space Science and Applications.

References

1. J. DEJACE, R. MATERA and G. PIATTI, *J. Mater. Sci. Lett.* **8** (1973) 754.
2. K. P. YOUNG and D. H. KIRKWOOD, *Metall. Trans.* **6A** (1975) 197.
3. C. M. KLAREN, J. D. VERHOEVEN and R. TRIVEDI, *ibid.* **11A** (1980) 1853.
4. J. T. MASON, J. D. VERHOEVEN and R. TRIVEDI, *J. Crystal Growth* **59** (1982) 516.
5. *Idem, Metall. Trans.* **15A** (1984) 1665.
6. P. N. QUESTED and M. McLEAN, *Mater. Sci. Engng* **65** (1984) 171.
7. Y. MIYATA, T. SUZUKI and J.-I. UNO, *Metall. Trans.* **16A** (1985) 1799.
8. S. N. TEWARI, *ibid.* **17A** (1986) 2279.
9. L. R. MORRIS and W. C. WINEGARD, *J. Crystal Growth* **1** (1967) 245.
10. T. OKAMOTO, K. KISHITAKE and I. BESSO, *ibid.* **29** (1975) 131.
11. D. J. ALLEN and J. D. HUNT, *Metall. Trans.* **7A** (1976) 767.
12. K. KOBAYASHI, Y. SEKO and P. SHINGU, *J. Jpn Inst. Metals.* **45** (1981) 647.
13. S.-C. HUANG and M. E. GLICKSMAN, *Acta Metall.* **29** (1981) 701.
14. *Idem, ibid.* **29** (1981) 717.
15. K. SOMBOONSUK, J. T. MASON and R. TRIVEDI, *Metall. Trans.* **15A** (1984) 967.
16. R. TRIVEDI and K. SOMBOONSUK, *Mater. Sci. Engng* **65** (1984) 65.
17. K. SOMBOONSUK and R. TRIVEDI, *Acta Metall.* **33** (1985) 1051.
18. H. ESAKA and W. KURZ, *J. Cryst. Growth* **72** (1985) 578.
19. M. A. CHOPA, M. E. GLICKSMAN and N. B. SINGH, *Metall. Trans.* **19A** (1988) 3087.
20. R. N. GRUGEL and Y. ZHOU, *ibid.* **20A** (1989) 969.
21. T. Z. KATTAMIS, J. C. COUGHLIN and M. C. FLEMINGS, *Trans. AIME* **239** (1967) 1504.
22. M. KAHLWEIT, *Scripta Metall.* **2** (1968) 251.
23. J. J. REEVES and T. Z. KATTAMIS, *ibid.* **5** (1971) 223.
24. N. J. WHISLER and T. Z. KATTAMIS, *J. Crystal Growth* **14** (1972) 20.
25. P. W. PETERSON, T. Z. KATTAMIS and A. F. GIAMEI, *Metall. Trans.* **11A** (1980) 1059.
26. M. BASARAN, *ibid.* **12A** (1981) 1235.
27. D. H. KIRKWOOD, *Mater. Sci. Engng* **73** (1985) L1.
28. A. MORTENSEN, *Metall. Trans.* **20A** (1989) 247.
29. B. BASU and J. A. SEKHAR, *ibid.* **20A** (1989) 1833.
30. E. HALDER and H. E. EXNER, *Acta Metall.* **36** (1988) 1665.
31. R. RIEDL and H. F. FISCHMEISTER, *Metall. Trans.* **21A** (1990) 264.
32. M. A. TAR, *Metal Sci.* January (1979) 9.
33. H. ESAKAL, PhD thesis, Ecole Polytechnique Federale de Lausanne, Switzerland, Thesis 615 (1986).
34. J. A. HORWATH and L. F. MONDOLFO, *Acta Metall.* **10** (1962) 1037.
35. P. K. ROHATGI and C. M. ADAMS Jr, *Trans. AIME* **239** (1967) 1737.
36. P. K. ROHATGI, S. M. JAIN, D. N. FRENCH and C. M. ADAMS Jr, *ibid.* **245** (1969) 267.
37. L. BÄCKERUD and B. CHALMERS, *ibid.* **245** (1969) 309.
38. F. WEINBERG and E. TEGHTSOONIAN, *Metall. Trans.* **3** (1972) 93.
39. G. R. KOTLER, K. W. CASEY, and G. S. COLE, *ibid.* **3** (1972) 723.
40. T. OKAMOTO and K. KISHITAKE, *J. Crystal Growth* **29** (1975) 137.
41. H. JACOBI and K. SCHWERDTFEGER, *Metall. Trans.* **7A** (1976) 811.
42. J. A. SPITTLE and D. M. LLOYD, in "Solidification and Casting of Metals", Book 192 (The Metals Society, 1979) pp. 15–20.
43. M. WOLF, T. W. CLYNE and W. KURZ, *Arch. Eisenhüttenw.* **3** (1982) 91.
44. H. M. TENSI and H. FUCHS, *Z. Metallkde* **74** (1983) 351.
45. *Idem., Geisserei-Forschung* **35** (1983) 61.
46. N. TUNCA and R. W. SMITH, *J. Mater. Sci.* **23** (1988) 111.
47. T. B. MASSALSKI (ed.) "Binary Alloy Phase Diagrams", (American Society for Metals, Metals Park, OH, 1986).
48. D. J. ALLEN and J. D. HUNT, *Metall. Trans.* **10A** (1979) 1389.
49. W. KURZ and R. N. GRUGEL, in "Solidification and microgravity", Materials Science Forum, 1991, ed. P. Bánczy (*Trans. Tech*, Switzerland, 1991) pp. 185–204.
50. R. M. SHARP and A. HELLAWELL, *J. Cryst Growth* **11** (1971) 77.

Received 7 August 1991
and accepted 7 April 1992